

# Modern nucleon-nucleon potentials and symmetry energy in infinite matter

L. Engvik<sup>a</sup>, M. Hjorth-Jensen<sup>b</sup>, R. Machleidt<sup>c</sup>, H. Mütter<sup>d</sup>, A. Polls<sup>e</sup>

<sup>a</sup> *Department of Physics, University of Oslo, N-0316 Oslo, Norway*

<sup>b</sup> *Nordita, Blegdamsvej 17, DK-2100 København Ø, Denmark*

<sup>c</sup> *Department of Physics, University of Idaho, Moscow, ID 83844, U.S.A.*

<sup>d</sup> *Institut für Theoretische Physik, Universität Tübingen, D-72076 Tübingen, Germany*

<sup>e</sup> *Departament d'Estructura i Constituents de la Matèria, Universitat de Barcelona, E-08028 Barcelona, Spain*

## Abstract:

We study the symmetry energy in infinite nuclear matter employing a non-relativistic Brueckner-Hartree-Fock approach and using various new nucleon-nucleon (NN) potentials, which fit np and pp scattering data very accurately. The potential models we employ are the recent versions of the Nijmegen group, Nijm-I, Nijm-II and Reid93, the Argonne  $V_{18}$  potential and the CD-Bonn potential. All these potentials yield a symmetry energy which increases with density, resolving a discrepancy that existed for older NN potentials. The origin of remaining differences is discussed.

## 1 Introduction

The equation of state (EOS) for neutron star matter and infinite nuclear matter has been intensively studied for many years. A correct description of the EOS would have far reaching consequences for topics ranging from the cooling of neutron stars [1,2] to the physics of heavy ion collisions [3]. Furthermore, recent radioactive ion beam experiments [4,5] have provided new information on the structure of unstable nuclei far from equilibrium. The latter may open the possibility of extracting information on the EOS for asymmetric matter

and the density dependence of the nuclear symmetry energy. The symmetry energy  $\mathcal{S}(n)$  is defined as the difference between the energy per particle in pure neutron matter  $\mathcal{E}(n, \chi_p = 0)$  and the binding energy per particle in symmetric nuclear matter  $\mathcal{E}(n, \chi_p = 1/2)$ , where  $n$  is the total baryon density in units of  $\text{fm}^{-3}$  and  $\chi_p = n_p/n$  is the proton fraction.

Knowledge of the symmetry energy at high densities is of particular importance in nuclear astrophysics where the density dependence of  $\mathcal{S}(n)$  is crucial for understanding e.g., the cooling mechanisms in a neutron star [2]. The symmetry energy determines the proton fraction in  $\beta$ -stable matter. The proton fraction is in turn important for the cooling history of a neutron star. At a certain critical value, typically  $\chi_p \approx 0.15$ , the so-called direct URCA processes for neutrino emissions are allowed [2]. Further, neutrino emissivity from the so-called modified URCA processes do also depend on the given proton fractions, see e.g., Ref. [6].

Many calculations of the symmetry energy and the EOS have been performed using different methods to solve the non-relativistic many-body problem of infinite nuclear matter and employing various realistic models of the nucleon-nucleon (NN) interaction, which were all adjusted to describe NN scattering phase shifts. All these calculations yield similar results for the symmetry energy around the saturation density of nuclear matter and are in reasonable agreement with the empirical estimate [1]. The predictions for the symmetry energies at high densities were quite different. The variational calculations of Wiringa et al. [7] using the Argonne  $V_{14}$  potential [8], predict e.g., a symmetry energy which varies only very little for densities  $n > 0.3 \text{ fm}^{-3}$ , while Brueckner-Hartree-Fock (BHF) calculations using One-Boson-Exchange potentials predict symmetry energies which increase with density also for larger densities [9,10].

This difference could be caused either by the method used to solve the many-body problem or by the NN interaction employed. Therefore, as a first step, we have recalculated the symmetry energy using the BHF approach described below and applied various realistic NN interactions. Results for these symmetry energies  $\mathcal{S}(n)$  as a function of density  $n$  are displayed in Fig. 1 for models of the NN interaction such as the Reid [11], Argonne  $V_{14}$  [8] and Paris potentials [12]. Using the Argonne  $V_{14}$  potential, the BHF calculation yields a symmetry energy which is almost constant for densities above twice nuclear matter density, consistent with results from corresponding variational calculations. The Reid potential leads to a symmetry energy which, at high densities, is even lower than the Argonne result, while the symmetry energy from the Paris potential increases almost linearly with density. These results indicate that the differences in the prediction of the symmetry energy at high densities are not caused by the many-body method used, but rather originates from the various models used for the NN interaction.

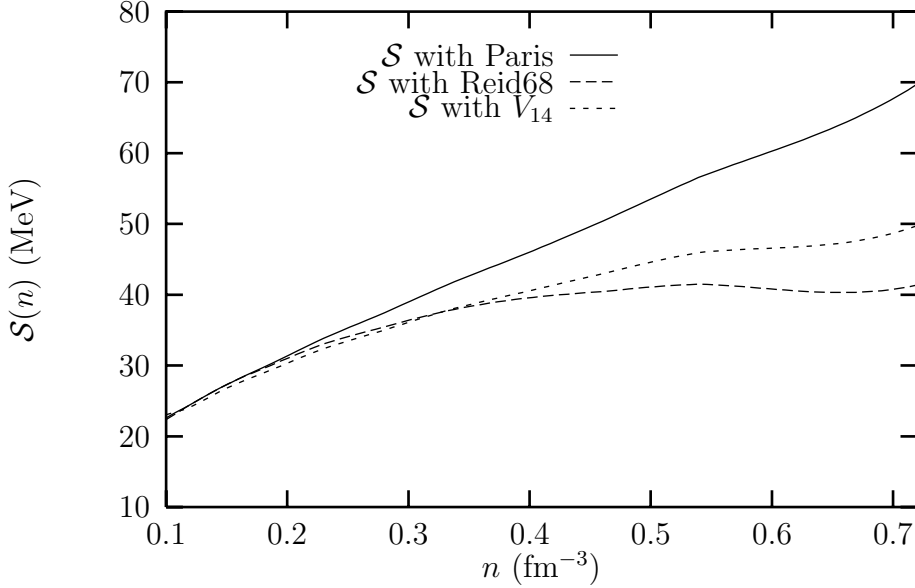


Fig. 1. Symmetry energy  $\mathcal{S}$  as function of density  $n$  for the Paris, Reid and Argonne  $V_{14}$  potentials.

A symmetry energy derived from the Reid or Argonne potential has in turn the consequence that the direct URCA process can never occur, or if it occurs, it starts at very high densities. For the  $V_{14}$  in a BHF calculation, it starts at a density of  $1.5 \text{ fm}^{-3}$ . This should be contrasted to the results with the Paris potential where the direct URCA process occurs at a density of  $0.9 \text{ fm}^{-3}$ .

However, when comparing these results, one should note that these potentials are not phase-shift equivalent, i.e., they do not predict exactly the same NN phases. Furthermore, the predicted phase shifts do not agree accurately with modern phase shift analyses, and the fit of the NN data is typically  $\chi^2/\text{datum} \approx 3$ . During the last years, progress has been made not only in the accuracy and the consistency of the phase-shift analysis, but also in the fit of realistic NN potentials to these data. As a result, several new NN potentials have been constructed which fit the world data for pp and np scattering below 350 MeV with high precision. Potentials like the recent CD-Bonn [13], the Argonne  $V_{18}$  [14] or the new Nijmegen [15] potentials yield a  $\chi^2/\text{datum}$  of about 1 and may be called phase-shift equivalent.

The aim of this paper is therefore to investigate whether these modern phase equivalent potentials also predict differences in the symmetry energy similar to those shown in Fig. 1. Moreover, we would like to trace possible different trends in the symmetry energy back to features of the NN potentials and their contributions in various partial waves. In order to do so, we will try to keep the many-body scheme as simple as possible. Here we will employ a non-relativistic BHF approach to evaluate the symmetry energy. In order to prepare the ground for studies of infinite matter, we present in the next section some results for the scattering matrix, while in section 3 we discuss

the symmetry energy for infinite matter. Concluding remarks are presented in section 4.

## 2 Phase-shift equivalent NN potentials

The potentials we will employ here are the recent models of the Nijmegen group [15], the Argonne  $V_{18}$  potential [14] and the charge-dependent Bonn potential (CD-Bonn [13]). In 1993, the Nijmegen group presented a phase-shift analysis of all proton-proton and neutron-proton data below 350 MeV with a  $\chi^2$  per datum of 0.99 for 4301 data entries. The above potentials have all been constructed based on these data. The CD-Bonn potential has a  $\chi^2$  per datum of 1.03 and the same is true for the Nijm-I, Nijm-II and Reid93 potential versions of the Nijmegen group [15]. The new Argonne potential  $V_{18}$  [14] has a  $\chi^2$  per datum of 1.09.

Although all these potentials predict almost identical phase shifts, their mathematical structure is quite different. The Argonne potential, the Nijm-II and the Reid93 potentials are non-relativistic potential models defined in terms of local potential functions, which are attached to various (non-relativistic) operators of the spin, isospin and/or angular momentum operators of the interacting pair of nucleons. Such approaches to the NN potential have traditionally been quite popular since they are numerically easy to use in configuration space calculations. The Nijm-I model is similar to the Nijm-II model, but it includes also a  $\mathbf{p}^2$  term, see Eq. (13) of Ref. [15], which may be interpreted as a non-local contribution to the central force. The CD-Bonn potential is based on the relativistic meson-exchange model of Ref. [16] which is non-local and cannot be described correctly in terms of local potential functions. However, it is represented most conveniently in terms of partial waves.

For a given NN potential  $V$ , the  $R$ -matrix (or  $K$ -matrix) for free-space two-nucleon scattering is obtained from the Lippmann-Schwinger equation, which reads in the center-of-mass (c.m.) system and in partial-wave decomposition

$$R_{l'l}^{JST}(q', q; E) = V_{l'l}^{JST}(q', q) + \sum_{l''} \mathcal{P} \int_0^\infty k^2 dk V_{l'l''}^{JST}(q', k) \frac{M}{ME - k^2} R_{l''l}^{JST}(k, q; E). \quad (1)$$

The label  $l$  represents the orbital angular momentum of the relative motion,  $J$  is the total angular momentum,  $S$  the spin and  $T$  the isospin. Relative momenta are given by  $q, q', k$ , while the energy of the interacting particles is denoted by  $E$ . Notice that the principle value integral ( $\mathcal{P}$ ) for the integration over the intermediate momenta  $k$  extends from zero to infinity. The phase-shifts for a given partial wave can be calculated from the on-shell matrix

element of  $R$ , which is obtained by setting

$$q = q' = q_0 \quad \text{and} \quad E = \frac{q_0^2}{M} \quad (2)$$

Since all NN interactions considered in this paper reproduce the same phase-shifts, the corresponding on-shell matrix elements of  $R$  calculated from these various potentials are identical as well. As an example, we display the value of these  $R$  matrix elements in Figs. 2 - 4 for NN scattering with  $T_{lab} = 2E = 150$  MeV and a corresponding value of  $q_0 = 265$  MeV/c. This  $R$  matrix element is denoted by a star and is identical for all 5 potentials under consideration. What is different, is the contribution of the first term on the right-hand side of Eq.(1) to this value of  $R$ , which is the Born approximation to  $R$ , and the contributions of second and higher order in  $V$ , which are contained in the second term on the right-hand side of Eq.(1). This is demonstrated in Figs. 2 - 4, which display the matrix elements  $V_{l'l}^{JST}(q_0, k)$  for the different bare potentials as a function of  $k$ . The diagonal matrix element  $V_{l'l}^{JST}(q_0, q_0)$ , which represents the Born approximation to the  $R$  matrix, is denoted by a solid dot.

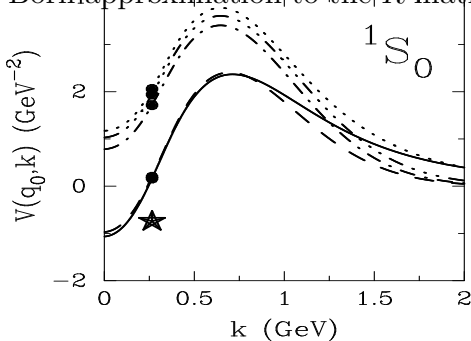


Fig. 2. Matrix elements  $V(q_0, k)$  for the  $^1S_0$  partial wave for the CD-Bonn (solid line), Nijm-I (dashed), Nijm-II (dash-dot), Argonne  $V_{18}$  (dash-triple-dot) and Reid93 (dotted) potentials. The diagonal matrix elements with  $k = q_0 = 265$  MeV/c (equivalent to  $T_{lab} = 150$  MeV) are marked by a solid dot. The corresponding matrix element of the full scattering  $R$ -matrix is marked by the star.

Looking e.g., at the results for the  $^3S_1$  channel displayed in Fig. 3 we see that the Nijm-II potential is a rather “hard” potential in the sense that the diagonal matrix element of the bare potential is very repulsive. In order to obtain the attractive matrix element of  $R$ , which yields the empirical phase shift, a lot of attraction has to be supplied from the contributions to  $R$  which are beyond the Born-approximation. On the other hand, the CD-Bonn potential is rather “soft” in this channel, implying that much less attraction is needed from the terms of higher order in  $V$  in Eq. (1), to obtain the empirical value of  $R$ .

Similar features can also be observed in the  $^1S_0$  and  $^3P_1$  partial waves in Figs.

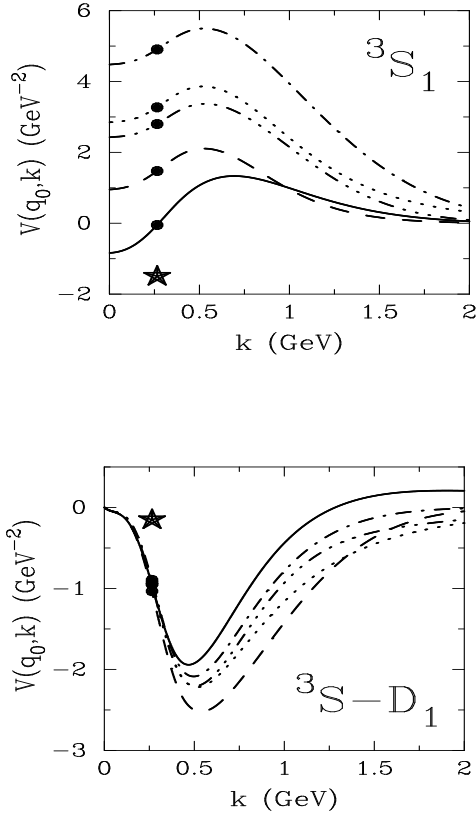


Fig. 3. Matrix elements for the  ${}^3S_1$  and  ${}^3S_1$ - ${}^3D_1$  potentials. Legend as in Fig. 2.

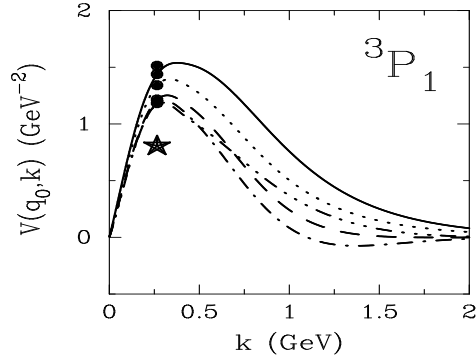


Fig. 4. Matrix elements for the  ${}^3P_1$  partial wave. Legend as in Fig. 2.

2 and 4, respectively. Different potentials turn out to be the “softest” potential in the various partial waves. It should be noted that the differences between the various potentials are getting smaller with increasing  $l$ . For  $D$ -waves and higher partial waves the various potentials are almost equal. There are still

differences for  $P$ -waves<sup>1</sup>.

So what are the differences between the various NN potentials discussed so far, which might be responsible for the differences displayed in Figs. 2 - 4? The NN potentials denoted by Reid93 and Nijm-II [15] are purely local potentials in the sense that they consider the local form of the One-Pion-Exchange potential for the long-range part and parametrize the contributions of medium and short-range in terms of local functions, depending on the distance between the interacting nucleons, multiplying a set of spin-isospin operators. The same is also true for the Argonne  $V_{18}$  potential [14]. The NN potential denoted as Nijm-I [15] also contains the local representation of the One-Pion-Exchange part but keeps track of non-localities of the medium- and short-range central-force components, which one obtains by evaluating these contributions from a One-Boson-Exchange model in terms of second-order Feynman diagrams. The CD-Bonn potential on the other hand [13] has been evaluated completely within this scheme. It has been shown [13] that ignoring the non-localities in the One-Pion-Exchange part leads to a larger tensor component in the bare potential. This may also be the origin of the fact that the CD-Bonn potential yields a smaller D-state probability for the Deuteron ( $P_D = 4.83\%$ ) than the other potentials ( $P_D \approx 5.6\%$ ).

Returning to Figs. 2 - 4 we see that for the  $^1S_0$  partial wave, which is not affected by the tensor component, the NN interactions CD-Bonn and Nijm-I, which both account for non-localities, exhibit rather similar results for the bare potential, while the pure local potentials do require more attraction from the non-Born terms to get to the empirical value of  $R$ . In the case of the  $^3S_1$  channel we observe a difference also between the CD-Bonn and the Nijm-I potential, which should be related to the fact that the CD-Bonn potential includes non-local effects also in the One-Pion-Exchange contribution. As it has been demonstrated in [13] the neglect of non-local components in the One-Pion-Exchange term increases the non-diagonal matrix elements of  $V$  in the coupling channel  $^3S_1$ - $^3D_1$  (cf. Fig. 3). This implies that the contributions to  $R$  in the  $^3S_1$  partial wave, which are of second and higher order in  $V$  (see Eq. 1), give rise to more attraction, when local approximations to One-Pion-Exchange term are considered. Consequently, the diagonal matrix elements of  $V$  in this channel must be less attractive to obtain the same matrix element for  $R$ . In the language used above this means that the potential which accounts for the non-locality of the One-Pion-Exchange (the CD-Bonn) is “softer” than the other potentials (see Fig. 3).

<sup>1</sup> The original Nijm-II potential yielded an unphysical bound state for the  $^1P_1$  wave, as pointed out by Nogga *et al.* [17]. In the present work, the updated Nijm-II potential is used [18].

### 3 Symmetry energy in infinite matter

The many-body method we will employ in deriving the symmetry energy and the relevant proton fractions is a rather simple one, the non-relativistic Brueckner-Hartree-Fock (BHF) method with a continuous single-particle spectrum [19]. Here it will serve us as a mere tool to investigate various NN potentials so that the discrepancies observed can be retraced to the NN potentials only. This is also the main aim of this work, as discussed in the introduction as well. Moreover, the  $G$ -matrix offers a rather direct link to the  $R$ -matrix discussed in the previous section. Therefore, as discussed below, eventual differences between various potentials in a finite medium should be easily retraced to e.g., Figs. 2-4 and the structure of the  $R$ -matrix.

Before we proceed, we feel however that a disclaimer is necessary. We do not, by obvious reasons, believe that a non-relativistic BHF scheme offers the most realistic approach to matter at densities above nuclear matter saturation density  $n = 0.17 \text{ fm}^{-3}$ . Other many-body contributions such as three-hole line contributions could be important in order to reproduce the empirical data. Although recent investigations by Baldo et al. [20] indicate that the BHF approach with a continuous choice for the single-particle spectrum accounts for three-hole line contributions in nuclear matter (see also the work of Day [21]), further many-body terms as included in the recent variational calculation of Akmal and Pandharipande [22]. Moreover, accounting only for nucleonic degrees of freedom should be viewed as nothing but a first approximation. There is no reason why other baryons should not be present at higher densities.

The energy per particle  $\mathcal{E}(n, \chi_p)$  within the BHF scheme is given in terms of the so-called reaction matrix  $G$ . The latter is obtained by solving the Bethe-Goldstone equation for various proton fractions  $\chi_p$  [9]

$$G(\omega, \chi_p) = V + V \frac{Q(\chi_p)}{\omega - H_0} G(\omega, \chi_p), \quad (3)$$

where  $\omega$  is the unperturbed energy of the interacting nucleons,  $V$  is the free NN potential,  $H_0$  is the unperturbed energy of the intermediate scattering states, and  $Q(\chi_p)$  is the Pauli operator preventing scattering into occupied states. Only ladder diagrams with intermediate two-particle states are included in Eq. (3). The structure of the Bethe-Goldstone equation can then be directly compared to the  $R$  matrix for free NN scattering, Eq. (1). Note that in (3) we have suppressed the quantum numbers for the various partial waves as well as the integral over the intermediate two-particle states in order to simplify the notation.

It is obvious that one expects the matrix elements of  $G$  to be rather close to those of  $R$  with only small deviations. These deviations originate from two



effects which reduce the contributions of second and higher order in  $V$  to the  $G$ -matrix as compared to their contributions to  $R$ . One is the so-called Pauli quenching effect: the Pauli operator  $Q$  in (3) restricts the intermediate particle states to states above the Fermi energy. The second one is the dispersive effect: the energy denominators in (3) are defined in terms of the single-particle energies of nucleons in the medium while the corresponding denominators of (1) are differences between the energies of free nucleons. Since the absolute values for the energy differences between nucleons, which feel the mean field of the nuclear system, are larger than the energy differences between the kinetic energies, also this dispersive correction reduces the attractive contributions of the non-Born terms.

As a result, the matrix elements of  $G$  tend to be less attractive than the corresponding matrix elements of  $R$ . This difference is due to the two quenching mechanisms which we just discussed. Since it originates from the quenching of the non-Born terms, it is smaller for a “soft” potential (using the terminology of the previous section) since the contribution of the non-Born term is weaker in this case. With the  $G$ -matrix we can calculate the total energy per nucleon

$$\mathcal{E}(n, \chi_p) = \mathcal{T} + \mathcal{U}(n, \chi_p), \quad (4)$$

with the kinetic energy

$$\mathcal{T} = \frac{3k_{Fp}^5 + 3k_{Fn}^5}{10m k_F^3} \quad (5)$$

where the total Fermi momentum  $k_F$  and the Fermi momenta  $k_{Fp}$ ,  $k_{Fn}$  for protons and neutrons are related to the total nucleon density  $n$  by

$$\begin{aligned} n &= \frac{2}{3\pi^2} k_F^3 \\ &= \chi_p n + (1 - \chi_p) n \\ &= \frac{1}{3\pi^2} k_{Fp}^3 + \frac{1}{3\pi^2} k_{Fn}^3 \end{aligned} \quad (6)$$

$\chi_p$  denotes the proton fraction and corresponds to the ratio of protons as compared to the total nucleon number ( $Z/A$ ). The contribution of the potential energy  $\mathcal{U}$  to the total energy per particle can be written

$$\mathcal{U}(n, \chi_p) = \frac{1}{2n} \frac{1}{(2\pi)^6} \sum_{a,b=(pn)} \int_0^{k_{Fa}} d^3 k_a \int_0^{k_{Fb}} d^3 k_b \langle k_a k_b | G(\omega = \epsilon_a(k_a) + \epsilon_b(k_b)) | k_a k_b \rangle, \quad (7)$$

The single-particle energies for protons and neutrons are denoted by  $\epsilon_a$ . For a given density  $n$  and proton fraction  $\chi_p$  they depend on the momentum  $k$  of the nucleon and are determined self-consistently using the BHF theory. The integrals in (7) can be decomposed into contributions of various partial waves. In the limit of pure neutron matter only those partial waves contribute, in which the pair of interacting nucleons is coupled to isospin  $T = 1$ . Due to

the antisymmetry of the matrix elements this implies that only partial waves with even values for the sum  $l + S$ , like  $^1S_0$ ,  $^3P_0$  etc. need to be considered in this case. For proton fractions different from zero, in particular the case of symmetric nuclear matter, also the other partial waves, like  $^3S_1 - ^3D_1$  and  $^1P_1$  contribute. See e.g. Ref. [23] for further details.

Since the contribution of the kinetic energy  $\mathcal{T}$  to the total energy is independent on the NN interaction chosen, we will restrict the following discussion to the potential energy per nucleon  $\mathcal{U}$  and explore the contribution of the various partial waves to it. As a first example we display in Fig. 5 the contribution of the  $^1S_0$  partial wave to the potential energy per nucleon  $\mathcal{U}$  of symmetric nuclear matter as a function of density  $n$ . The potentials employed are the CD-Bonn potential [13](solid line), the three Nijmegen potentials, Nijm-I (long dashes), Nijm-II (short dashes) and Reid93 (dotted line)[15] and the Argonne  $V_{18}$  [14] (dot-dashed line).

One observes that the results for the CD-Bonn potential are essentially identical to those of the Nijm-I. Both potentials yield substantially more attraction in this particular partial wave than the other three considered here. This is in complete agreement with the observations made in the previous section (see Fig. 2). There we observed that the CD-Bonn and the Nijm-I potential, the two potentials accounting for non-local effects in the medium- and short-range components of the central force are “softer” in this partial wave than the other two. This means that the quenching effects, which reduce the attraction of the non-Born terms in  $G$  as compared to  $R$  (as discussed above) are less efficient for these two potentials as compared to Nijm-II, Reid93 and Argonne  $V_{18}$ . Consequently the CD-Bonn potential and the Nijm-I yield more attraction. At a density of e.g.,  $0.6 \text{ fm}^{-3}$ , we get a contribution to the potential energy from the  $^1S_0$  channel of  $-33.4$ ,  $-33.2$ ,  $-29.2$ ,  $-29.1$  and  $-29.1$  MeV for the CD-Bonn, Nijm I, Nijm II, Reid93 and Argonne potentials, respectively.

Similar observations can also be made for the contribution of the  $^3S_1$  partial wave to the binding energy per nucleon displayed in Fig. 6. The “softer” the potential in this channel (compare Fig. 3), the more attraction is obtained. Although the differences we observed in the previous figure for the  $^1S_0$  wave are present here as well, this partial wave is particularly sensitive to the tensor component of the NN interaction, which originates mainly from the One-Pion-Exchange contribution. Due to these strong tensor correlations, the non-Born terms in Eqs. (1) and (3) are more important in the  $^3S_1$  than in the  $^1S_0$  channel. Therefore, the differences in the binding energy contribution predicted from the different interactions are particularly large in this channel. A potential model with a weak tensor force yields more attraction in a nuclear system than a potential with a strong tensor force. This is clearly seen in Fig. 6 where we study the contribution from the  $^3S_1$  partial wave in the contribution to the potential energy  $\mathcal{U}$ . At a density of  $0.6 \text{ fm}^{-3}$ , we get a contribution

to the potential energy from the  ${}^3S_1$  channel of  $-33$ ,  $-24$ ,  $-20.4$ ,  $-21.3$  and  $-20.1$  MeV for the CD-Bonn, Nijm I, Nijm II, Reid93 and Argonne potentials, respectively, a difference of more than 50% between the CD-Bonn potential and the Nijm II, Reid93 and Argonne potentials. However, it is not only the tensor which plays a significant role in explaining the differences seen in Figs. 5 and 6. The Nijm I potential has a non-local term to the central force, a term which explains the differences of approximately 20% between the Nijm I potential and the Nijm II and Reid93 potentials. This is the same mechanism discussed in connection with Fig. 5. The non-localities included in the tensor force of the CD-Bonn potential are in turn responsible for the further difference of 9 MeV between the CD-Bonn potential and the Nijm I potential. The differences discussed in Fig. 3 and the way they affect the integral term in the  $G$ -matrix (and  $T$ ) are clearly seen in Fig. 6.

Thus, Figs. 5 and 6 demonstrate in a clear way the importance of the tensor force and non-local terms in the construction of the nucleon-nucleon force. In addition, non-negligible differences seen in  $P$ -waves are reflected in different behaviors for partial waves with  $l \geq 1$ . In Fig. 7 we display the contributions from partial waves with  $l \geq 1$ . In the  $P$  channels, the CD-Bonn potential predicts less attraction than the other potentials. This in line with the observation made in the previous section (see Fig. 4) that for these partial waves, the Nijmegen potentials are “softer”. Note also that the Argonne  $V_{18}$  slightly deviates from the Nijmegen potentials. The difference can mainly be retraced to different contributions from  $P$ -waves. This difference, together with that observed in the  ${}^1S_0$  channel of Fig. 5, will be important in explaining the behavior of the new Argonne potential in neutron matter. For partial waves with  $l \geq 2$ , the results differ by some few keV only.

Putting the contributions from various channels together<sup>2</sup>, one obtains the total potential energy per nucleon  $\mathcal{U}$  for symmetric nuclear matter and neutron matter. These results are displayed in Figs. 8 and 9, respectively.

The differences between the various potentials are larger in calculating the energy of nuclear matter. This is mainly due to the importance of the  ${}^3S_1 - {}^3D_1$  contribution as we discussed above. This is of course in line with previous investigations, which showed that the predicted binding energy of nuclear matter is correlated to the strength of the tensor force, expressed in terms of the D-state probability obtained for the deuteron (see e.g. [23]). This importance of the strength of the tensor force is also seen in the calculation of the binding energy of the triton in Ref. [13,17]. The CD-Bonn potential yields a binding energy of 8.00 MeV, the Nijm-I potential gives 7.72 MeV while the Nijm-II yields 7.62 MeV, the same as does the new Argonne potential [14].

<sup>2</sup> In our calculations we include all partial waves with  $l < 10$ .

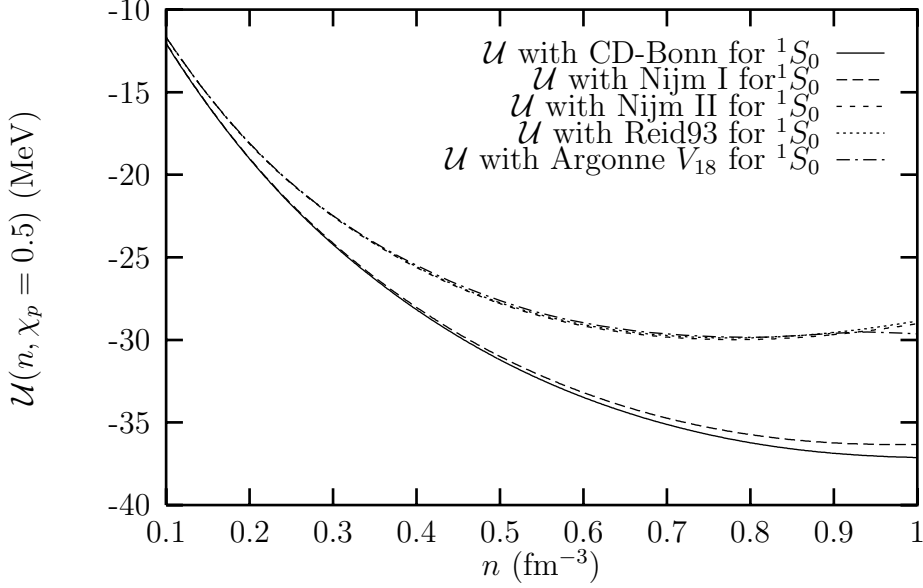


Fig. 5. Potential energy per particle  $\mathcal{U}$  for symmetric nuclear matter originating from the  $^1S_0$  partial wave only as a function of density  $n$ . Results are shown for the CD-Bonn potential [13], the new Argonne  $V_{18}$  potential [14] and the three recent versions of the Nijmegen group [15].

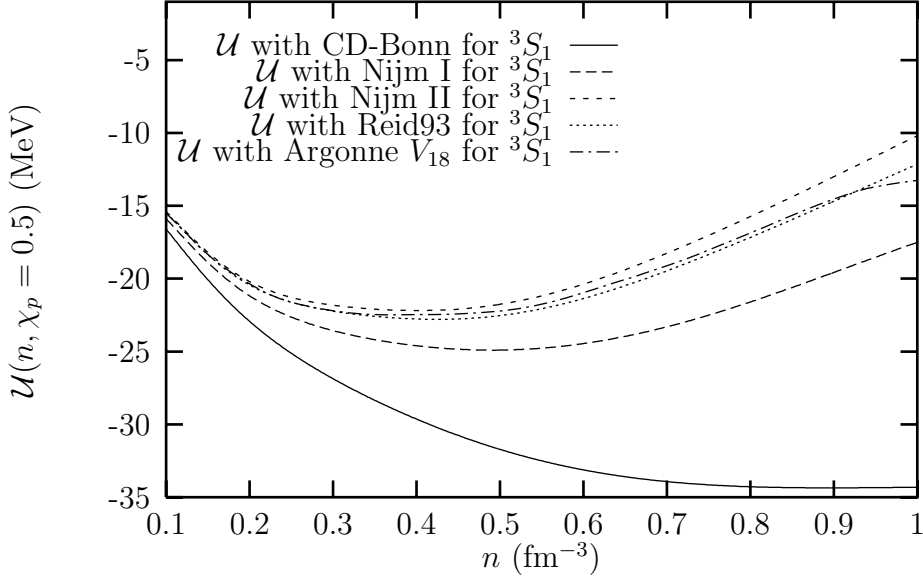


Fig. 6. Potential energy per particle  $\mathcal{U}$  for symmetric nuclear matter originating from the  $^3S_1$  partial wave only.

In Fig. 9 we have plotted the results for pure neutron matter. For the density of  $0.6 \text{ fm}^{-3}$ , we get a contribution to the potential energy of  $-29.0$ ,  $-30.2$ ,  $-28.7$ ,  $-28.1$  and  $-24.0$  MeV for the CD-Bonn, Nijm I, Nijm II, Reid93 and Argonne potentials, respectively, i.e., a difference of the order of few percents for the first four potentials. The Argonne  $V_{18}$  potential [14] deviates from the other four potentials due to slightly more repulsive contributions from  $P$ -

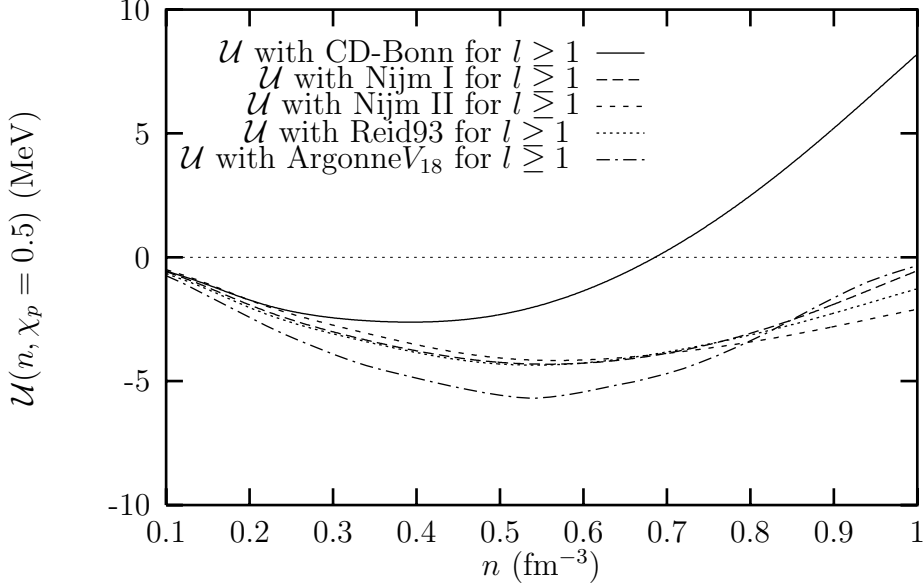


Fig. 7. Potential energy per particle  $\mathcal{U}$  for symmetric nuclear matter originating from partial waves with  $l \geq 1$ .

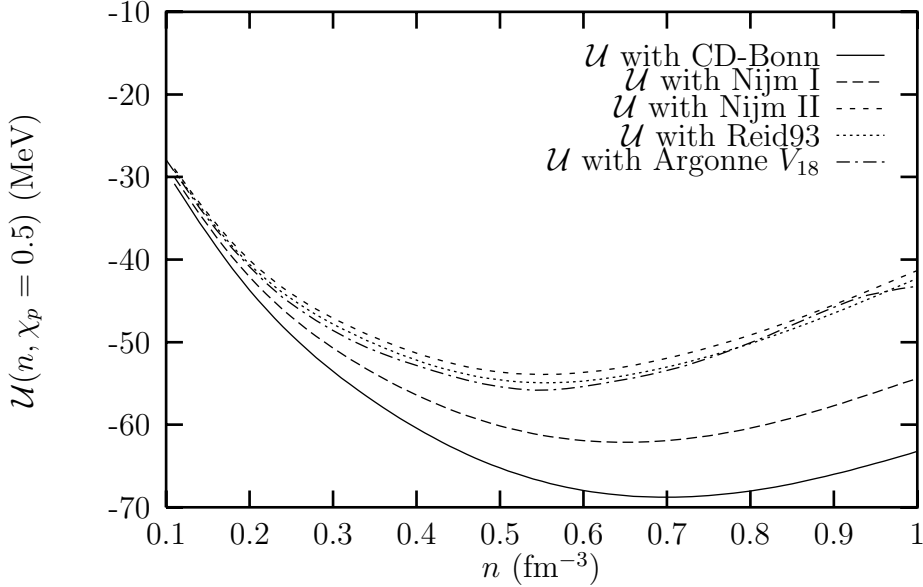


Fig. 8. Potential energy per particle  $\mathcal{U}$  for symmetric nuclear matter as function of total baryonic density  $n$ .

waves, especially from the  ${}^3P_1$  wave. Similar results were also obtained recently in Ref. [22] for the new Argonne potential. In the  $T = 1$  channel there are no contributions from the  ${}^3S_1$  channel and the tensor force plays therefore a less important role. The differences in the  ${}^1S_0$  channel follow the discussion above in connection with Fig. 5. Further differences are mainly due to contributions from the  ${}^3P_1$  partial wave.

From the potential energy  $\mathcal{U}$  one can evaluate the total energy per nucleon

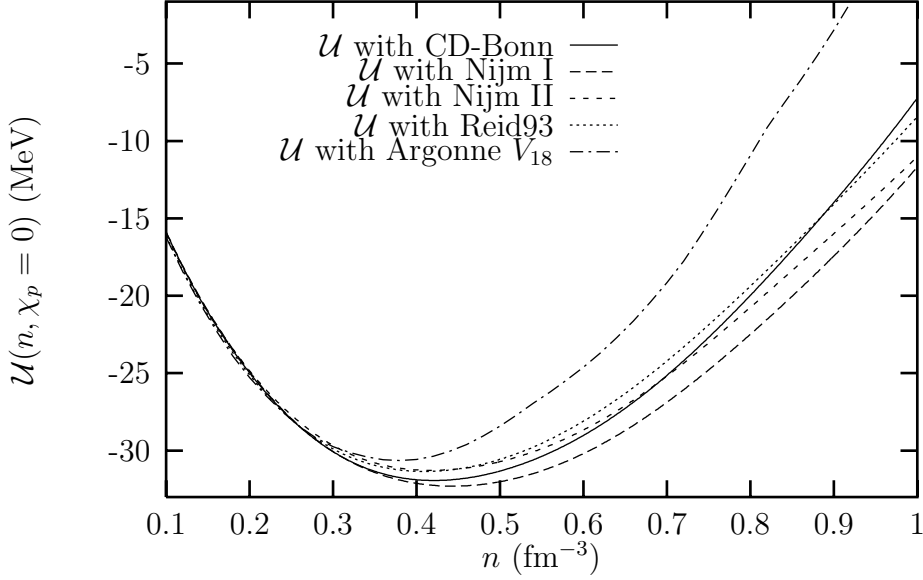


Fig. 9. Potential energy per particle  $\mathcal{U}$  for pure neutron matter.

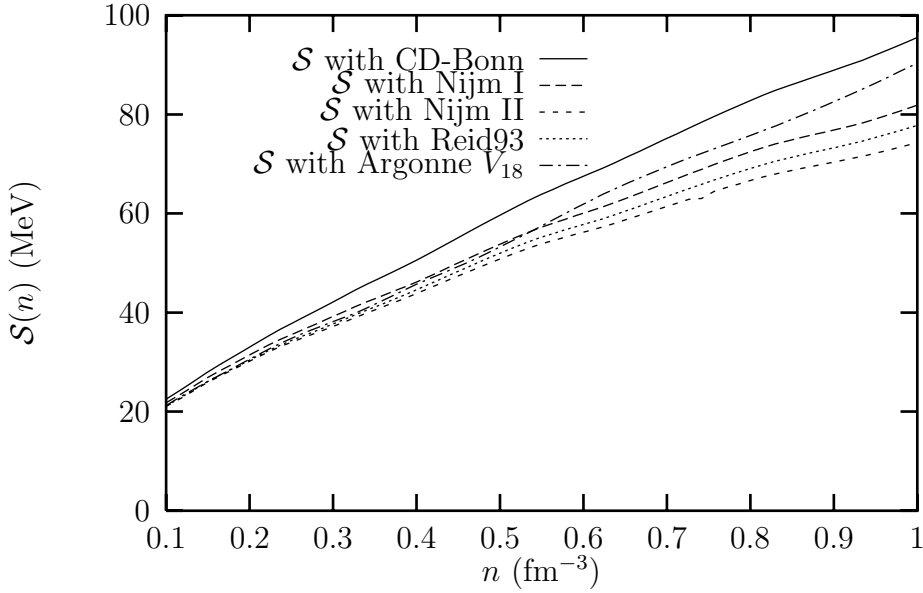


Fig. 10. Symmetry energy  $\mathcal{S}$  as function of density  $n$ .

$\mathcal{E}$  according to Eq. (4) for both symmetric nuclear matter and pure neutron matter and identify the difference with the symmetry energy

$$\mathcal{S}(n) = \mathcal{E}(n, \chi_p = 0) - \mathcal{E}(n, \chi_p = 1/2) \quad (8)$$

Results for these symmetry energies as a function of density  $n$  are presented in Fig. 10. None of the new potentials predict a saturation of the symmetry energy as a function of density as was the case for older local potentials discussed in Fig. 1. The differences between the various predictions are smaller than those between the older versions of the NN potential. The remaining discrepancies can be traced back to the non-locality of the potential considered, as

we discussed above. For the Argonne potential, where the results in symmetric nuclear matter are almost identical to those from the Reid93 and the Nij II potentials (see e.g., Fig. 3) the increase is mainly due to the abovementioned more repulsive contributions from  $P$ -waves in neutron matter.

From the differences in symmetry energies one would expect that properties like proton fractions in  $\beta$ -stable matter will be influenced. This in turn has consequences for the cooling history of a neutron star. Thus, for the sake of completeness, we show in Fig. 11 resulting proton fractions in  $\beta$ -stable matter. The proton fraction in  $\beta$ -equilibrium is determined by imposing the relevant equilibrium conditions on the processes  $e^- + p \rightarrow n + \nu_e$  and  $e^- \rightarrow \mu^- + \bar{\nu}_\mu + \nu_e$ . The conditions for  $\beta$ -equilibrium require that  $\mu_n = \mu_p + \mu_e$ , where  $\mu_i$  is the chemical potential of particle species  $i$ , and that charge is conserved  $n_p = n_e$ . We include muons, which appear at densities close to the saturation density for nuclear matter. We assume that the neutrinos do not contribute. The proton and neutron chemical potentials are determined from the energy per particle  $\mathcal{E}(n, \chi_p)$  where we calculate the latter quantity for several proton fractions  $\chi_p$  and impose the above equilibrium conditions for  $\beta$ -stable matter.

It is seen from Fig. 11 that the differences reflected in the symmetry energy appear also for the proton fractions. For the CD-Bonn potential the direct URCA process can occur at a density of  $0.88 \text{ fm}^{-3}$ , for the Nijm I it starts at  $1.25 \text{ fm}^{-3}$  while for the Reid93 potential one reaches the critical density at  $1.36 \text{ fm}^{-3}$ . The Argonne potential allows for the direct URCA process at a density of  $1.05 \text{ fm}^{-3}$ . For the Nijm II we were not able to get the direct URCA process for densities below  $1.5 \text{ fm}^{-3} \text{ MeV}$ .

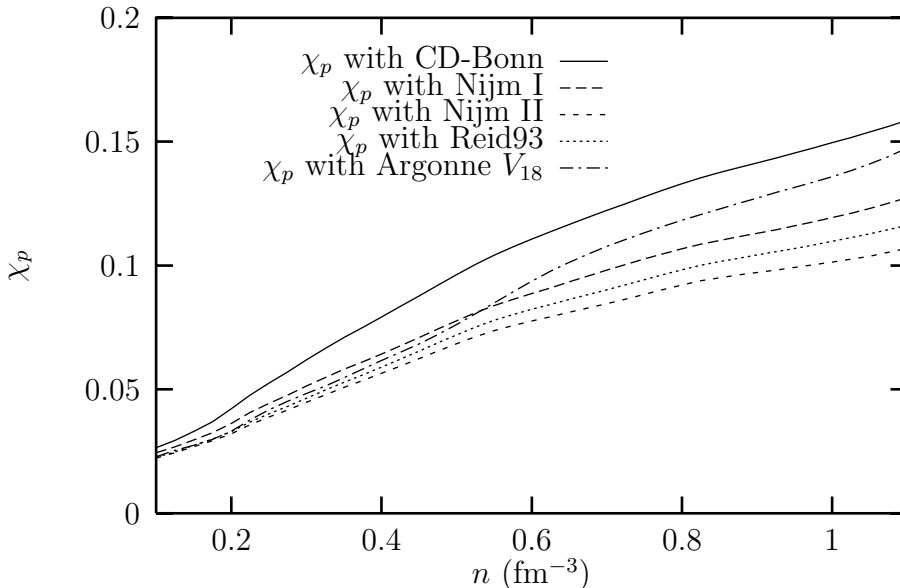


Fig. 11. Proton fraction  $\chi_p$  for  $\beta$ -stable matter as function of density  $n$

Finally, in Fig. 12 we plot the final equation of state  $\varepsilon$  (which also includes the contribution from leptons) for  $\beta$ -stable matter. Since the proton fractions are not too large, see Fig. 11, the  ${}^3S_1$  contribution with  $T_z = 0$  plays a less significant role than that seen in Fig. 6. Thus, the main contribution to the differences between the various potentials arises from the  $T_z = 1$  channel. The

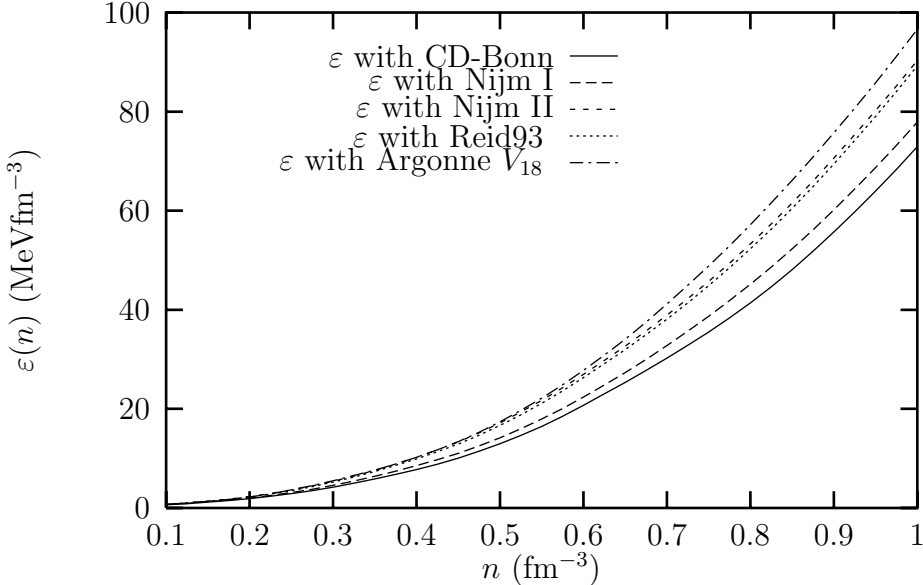


Fig. 12. Equation of state  $\varepsilon$  for  $\beta$ -stable matter as function of density  $n$

results for  $\beta$ -stable matter shown in Fig. 12 are gratifying in the sense that with the present high-quality potentials one does not have the large differences between potentials as seen e.g. in Ref. [7]. This means also that a calculation like the present with two-body forces only and employing new high-quality potentials will yield a mass-radius relationship for a neutron star which is rather similar for all potentials considered.

## 4 Conclusions

The most recent parametrizations of the nucleon-nucleon potential have been employed to evaluate the energy of asymmetric nuclear matter at high densities using the non-relativistic Brueckner-Hartree-Fock (BHF) approximation. An attempt has been made to relate the differences in the predicted energies to basic features of these interactions which are essentially phase-shift equivalent.

We find that the energies predicted for pure neutron matter and  $\beta$ -stable matter are quite similar for all modern NN potentials. This may indicate that inconsistencies between various models for the NN potential in the isospin  $T = 1$  channel have been diminished by the improved fit to the data. Differences are larger for the calculated energy of symmetric nuclear matter. All symmetry



energies resulting from the different potentials increase with density, no saturation is observed, as was the case for older models of the NN potential[8,11]. The remaining discrepancies can be traced back to the inclusion of non-local contributions in the short-range components of the NN interaction as well as in the One-Pion-Exchange contribution. The non-localities included in the CD-Bonn potential[13] and partly also in the Nijm-I potential of the Nijmegen group[15] lead to more binding energy in nuclear matter. These non-localities are based on the meson-exchange model of the NN interaction. Their inclusion may be considered as an improvement compared to purely local potentials like Nijm-II, Reid93 and Argonne  $V_{18}$ [14]. Additional non-local contributions may arise from short-range quark-gluon exchange.

The calculations have been performed using a simple many-body scheme, a non-relativistic Brueckner-Hartree-Fock approach. The reason being that this method allows one in a direct way to relate certain many-body terms directly to the  $T$ -matrix. More complicated many-body terms have to be included in order to obtain a realistic EOS and symmetry energy. Three-body forces [7,22] and/or relativistic effects [9] are known to add repulsion at higher densities. These effects may therefore yield a more repulsive EOS and stiffer symmetry energy.

## Acknowledgement

This work was supported in part by The Research Council of Norway (Programme for Supercomputing) through a grant for computing time and by the U.S. National Science Foundation through Grant No. PHY-9603097. Many discussions with Marcello Baldo, Fiorella Burgio, Øystein Elgarøy, Eivind Osnes, Vijay Pandharipande, Steven Pieper, Angels Ramos and Robert Wiringa are greatly acknowledged. This work has been completed at the European Centre for Theoretical Nuclear Physics and Related Areas, ECT\*, Trento, Italy. We acknowledge the hospitality of the ECT\*.

## References

- [1] C.J. Pethick and D.G. Ravenhall, *Annu. Rev. Nucl. Part. Phys.* 45 (1995) 429.
- [2] M. Prakash, *Phys. Rep.* 242 (1994) 191.
- [3] B.-A. Li, C.M. Ko and Z. Ren, *Phys. Rev. Lett.* 78 (1997) 1644.
- [4] I. Tanihata, *Prog. Part. Nucl. Phys.* 35 (1995) 505.

- [5] P.G. Hansen, A.S. Jensen and B. Jonson, *Annu. Rev. Nucl. Part. Sci.* 45 (1995) 591.
- [6] B.L. Friman and O.V. Maxwell, *Ap. J.* 232 (1979) 541.
- [7] R.B. Wiringa, V. Fiks and A. Fabrocini, *Phys. Rev. C* 38 (1988) 1010.
- [8] R.B. Wiringa, R.A. Smith and T.L. Ainsworth, *Phys. Rev. C* 29 (1984) 1207.
- [9] L. Engvik, E. Osnes, M. Hjorth-Jensen, G. Bao and E. Østgaard, *Ap. J.* 469 (1996) 794.
- [10] M. Baldo, G.F. Burgio and I. Bombaci, submitted to *Phys. Rev. Lett.*
- [11] R.V. Reid, *Ann. Phys.* 50 (1968) 411.
- [12] M. Lacombe *et al*, *Phys. Rev. C* **21**, 861 (1980).
- [13] R. Machleidt, F. Sammarruca and Y. Song, *Phys. Rev. C* 53 (1996) R1483.
- [14] R.B. Wiringa, V.G.J. Stoks and R. Schiavilla, *Phys. Rev. C* 51 (1995) 38.
- [15] V.G.J. Stoks, R.A. M. Klomp, C.P.F. Terheggen and J.J. de Swart, *Phys. Rev. C* 49 (1994) 2950.
- [16] R. Machleidt, *Adv. Nucl. Phys.* 19 (1989) 185.
- [17] A. Nogga, D. Hüber, H. Kamada and W. Glöckle, preprint nucl-th/9704001.
- [18] V.G. J. Stoks, private communication.
- [19] J.P. Jeukenne, A. Lejeune and C. Mahaux, *Phys. Rep.* 25 (1976) 83; C. Mahaux, P.F. Bortignon, R.A. Broglia and C.H. Dasso, *Phys. Rep.* 120 (1985) 1.
- [20] M. Baldo, contribution to “International Workshop on Microscopic Many-Body Methods”, ECT\*, Trento, Italy (May 26-june 6, 1997).
- [21] B.D. Day, *Phys. Rev. C* 24 (1981) 1203.
- [22] A. Akmal and V.R. Pandharipande, preprint nucl-th/9705013 and submitted to *Phys. Rev. C*.
- [23] M. Hjorth-Jensen, T.T.S. Kuo and E. Osnes, *Phys. Rep.* 261 (1995) 125.